Nonreciprocal pulse shaping and chaotic modulation with asymmetric noninstantaneous nonlinear resonators

A. Hofstrand,[1] M. Cotrufo,[1] and A. Alù[1,2]
[1]*Photonics Initiative, Advanced Science Research Center, City University of New York, New York 10031, USA*
[2]*Physics Program, Graduate Center, City University of New York, New York, NY 10016, USA*

(Received 11 August 2021; revised 25 October 2021; accepted 28 October 2021; published 29 November 2021)

Electromagnetic nonlinearity, combined with symmetry breaking, can be exploited to obtain highly nonreciprocal light transmission. In previous studies on nonreciprocity, it has been generally assumed that the material's nonlinearity responds instantaneously to the applied field. Here, we consider a noninstantaneous nonlinear response and study its influence on nonreciprocity. We show that the inclusion of such delayed effects can lead to highly nontrivial nonreciprocal dynamics, which are forbidden in the instantaneous regime. Particularly, when the characteristic delay time of the nonlinearity approaches the input pulse's duration, high-contrast nonreciprocal compression and reshaping of the pulse can be achieved. In the high-power regime, we show that it is possible to generate a nonreciprocal response in a single resonator, which, for instance, is chaotic when sourced along one direction and periodically modulated when sourced from the opposing direction. Indeed, by tuning the nonlinearity's memory time we can flexibly control the system's response, enabling a wide range of nonreciprocal functionalities in compact, passive, and bias-free devices.

DOI: 10.1103/PhysRevA.104.053529

I. INTRODUCTION

Achieving unidirectional light transmission is a major goal in developing photonic technologies, but in many standard scenarios it is forbidden by the Lorentz reciprocity theorem (LRT) [1]: In any electromagnetic system whose permittivity and permeability tensors are symmetric, time invariant, and linear, light transmission between a source and a detector is the same when their locations are interchanged. In order to break reciprocity at least one of the assumptions of the LRT must be violated. The most common approach involves applying a dc magnetic bias to magneto-optical materials [2,3], but its implementation in integrated circuits is hindered by the need for large magnetic fields. Time-varying materials can also be used to break reciprocity without the need for magnetic fields [4–10], but the resulting devices require complex modulation networks, and suffer trade-offs between the footprint, modulation features, and operational bandwidth [10].

As an alternative approach, nonlinearity-based methods have raised significant attention in recent years, offering a path towards bias-free, fully passive nonreciprocity in nanoscale devices [11]. Among the various types of nonlinearities, Kerr-like responses, in which the material permittivity depends linearly on the local field intensity, are the most commonly investigated and utilized due to their ubiquity in optics [12]. By combining a nonlinear material with tailored spatial symmetry breaking, the same signal, injected from opposite directions, induces different field distributions that in turn create different intensity-dependent permittivity profiles, and thus break reciprocity [11]. Interestingly, no external bias is required in this approach, since the system is "self-biased" by the input field. Due to its simplicity, this approach has been successfully demonstrated in vastly different frameworks, such as integrated Si [13,14] and InP [15] microcavities operating in the near infrared, microwave circuits [16], and asymmetric azobenzene compounds [17]. Theoretical proposals have demonstrated free-space nonreciprocity via single [18,19] and cascaded [20,21] metasurfaces. Similar phenomena have also been demonstrated in quantum systems [22,23], where the nonlinearity is due to the saturable response of atoms. In all of the mentioned studies, the nonlinearity is assumed to have a negligible buildup time: Upon application of an electric field $\mathbf{E}(\mathbf{r})$, the permittivity at each point $\mathbf{r}$ changes *instantaneously* from its low-intensity value $\varepsilon_{\text{lin}}(\mathbf{r})$ to $\varepsilon(\mathbf{r}) = \varepsilon_{\text{lin}}(\mathbf{r}) + \varepsilon_0\chi^{(3)}|\mathbf{E}(\mathbf{r})|^2$. Thus, the resonant frequency and/or linewidth of a resonator filled with such a material are instantaneously affected as the intracavity power changes. Importantly, this instantaneous assumption implies that the system still obeys time-reversal (TR) symmetry, which is known to lead to bounds between the nonreciprocal power bandwidth and insertion loss [18]. The instantaneous approximation is well justified in many practical scenarios: For example, the characteristic buildup time of the optical Kerr effect is less than 10 fs in silicon [24], much smaller than any other relevant timescale. However, there exist nonlinearities with more pronounced memory effects and buildup times. The thermoelectric effect in liquids, for example, has a buildup time as large as tens of μs [25,26], and recent studies have employed such delayed nonlinearities in oil-filled cavities [25,26]. Importantly, such slow buildup times can approach or even surpass the relevant timescales of the system, such as the pump pulse's temporal width or the lifetime of the hosting resonator. Notably, a nonzero buildup time manifestly breaks TR symmetry,

since upon time inversion the nonlinearity-induced permittivity change precedes the input pulse, violating causality.

This fundamental difference between instantaneous and noninstantaneous nonlinear responses, and the associated relation with TR symmetry, raises the intriguing question of whether and how a temporal delay in the nonlinear response affects the nonreciprocal response, and whether different functionalities can be obtained. As we show, introducing a delay in the nonlinear response leads to phenomena not observable in the instantaneous regime, such as nonreciprocal self-induced oscillations, pulse compression, and reshaping. A general theory of self-oscillatory behavior due to noninstantaneous responses, such as those caused by interactions with free carriers and thermal effects in photonic cavities, has been developed in Refs. [27–29]. Here, the goal is to investigate whether such behavior can be induced in nonlinear devices with structural asymmetries, leading to nonreciprocal signal modulation. Furthermore, it is known that the inclusion of delayed responses in optical cavities can lead to deterministic chaos [30,31]. A chaotic modulation in laser outputs has a number of appealing applications, including sensing of a weak coherent radiation source masked by a large incoherent background [32], random-bit generation [33], and securing optical communications [34]. A few previous works have considered inducing nonreciprocal chaos [35,36]. In contrast to these works, here we explore the opportunity of inducing a chaotic output with a delayed nonlinearity in a single resonator. By calculating the period-doubling bifurcation diagram, we also show the conditions under which our system can exhibit chaotic output for excitation along one direction and nonchaotic output in the opposite direction, when being excited by the same source. Having directional control over a chaos-induced signal would add important functionalities to the encryption and sensing applications mentioned above. The paper is organized as follows: In Sec. II we give the details of our model; in Sec. III we present analytical and numerical results, highlighting nonreciprocal functionality which is only possible with the inclusion of delayed nonlinear responses; in Sec. IV we give some concluding remarks.

II. MODEL DESCRIPTION

We begin by considering a resonator supporting a single mode with bare frequency ω_0, loaded with a Kerr-like nonlinearity and connected to two external input/output ports [see Fig. 1(a)]. The resonator energy decays into the two ports with rates γ_j $(j = 1, 2)$ and, neglecting any other decay channels, the total decay rate is $\gamma \equiv \gamma_1 + \gamma_2$. Employing coupled-mode theory (CMT) with conveniently normalized quantities (see Appendix), including time normalized in units of γ^{-1}, the resonator dynamics are described by the adimensional amplitude $a(t)$ given by the equations

$$\dot{a}(t) = \{i[\Delta - n(t)] - 1\}a(t) + \sqrt{2}\sum_{j=1,2}\mu_j\xi_j^+(t), \quad \text{(1a)}$$

$$\tau\dot{n}(t) = |a(t)|^2 - n(t), \quad \text{(1b)}$$

where $\xi_j^+(t)$ is the envelope of the input field from the jth port, and $\Delta \equiv (\omega - \omega_0)/\gamma$ is the detuning of the input carrier frequency, ω. The complex coefficients μ_j quantify the coupling between input fields and the resonator, and satisfy $|\mu_j|^2 = \gamma_j/\gamma$. The system is *electromagnetically asymmetric* if it couples to the two ports differently, i.e., $\gamma_1 \neq \gamma_2$ [11]. The time-dependent adimensional detuning $n(t)$ is induced by the Kerr-like nonlinearity with a characteristic buildup time τ. Such a model is commonly used to describe delayed nonlinear responses, e.g., Refs. [25,31,37,38]. The noninstantaneous nature of the nonlinearity in (1) is seen by formally integrating (1b), giving

$$n(t) = \frac{1}{\tau}\int_{-\infty}^{t} e^{-(t-s)/\tau}|a(s)|^2 ds, \quad (2)$$

where the temporal nonlocality of the response is explicitly expressed as a convolution with an exponentially decaying kernel. Importantly, Eq. (2) shows that system (1) is not, in general, symmetric under TR for finite $\tau > 0$. Only when the delay becomes negligible ($\tau \to 0$) does the kernel function in (2) formally approach the Dirac delta distribution and TR symmetry is restored. Note that the steady-state solution $[\dot{a}(t), \dot{n}(t)] = [0, 0]$ of (1) under cw pumping and for a finite delay τ is formally equivalent to the steady-state solution obtained in the instantaneous case. However, and quite importantly, the noninstantaneous nature of the nonlinearity can drastically alter the system's stability around these

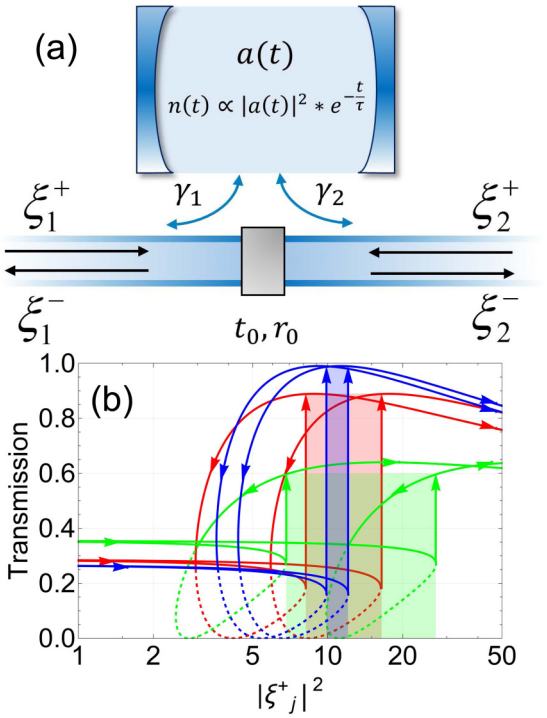

FIG. 1. (a) Schematic of the system considered in the text: An asymmetric single resonator is side coupled to a waveguide. (b) The port-to-port transmissions T_{12} and T_{21} (defined in the text) at steady state with cw pumping vs injected power for $\tau = 0$, $\Delta = 4$, $r_0 = 1/\sqrt{2}$, and increasing asymmetry $\gamma_2/\gamma_1 = 11/9$ (blue), $\gamma_2/\gamma_1 = 2$ (red), and $\gamma_2/\gamma_1 = 4$ (green) (grayscale: dark to light). The NRIR is highlighted by the shaded area and the arrows indicate hysteresis as a function of injected power due to the bistability of the steady-state solutions. The stable (unstable) portions of the curves are solid (dashed).

steady-state solutions. Regions of linear instability about steady states can lead to dynamic asymptotic responses such as stable limit cycles. Also, the evolution of $a(t)$ and $n(t)$ in system (1) can even become chaotic [31,39] in the highly detuned regime, which is discussed further below.

The possible nonreciprocity arising in our system, schematically shown in Fig. 1, can be described by calculating the port-to-port transmissions $T_{ij} \equiv |\xi_i^-|^2/|\xi_j^+|^2$ $(i, j = 1, 2)$, where $\boldsymbol{\xi}^- \equiv [\xi_1^-, \xi_2^-]^\mathsf{T}$ are the outgoing fields. These are related to the input fields $\boldsymbol{\xi}^+ \equiv [\xi_1^+, \xi_2^+]^\mathsf{T}$ and the cavity field via the linear relation $\boldsymbol{\xi}^- = \sqrt{2}[\mu_1, \mu_2]^\mathsf{T} a + \mathbf{M}\boldsymbol{\xi}^+$, where $\mathbf{M} \equiv [r_0, it_0; it_0, r_0]$ and r_0 and t_0 are the transmission and reflection coefficients $(t_0^2 + r_0^2 = 1)$ of the system when excited far off resonance. In the linear case, the following constraints on our system's parameters can be derived from general time-reversibility and energy conservation arguments (see Ref. [40]),

$$\begin{pmatrix} r_0 & it_0 \\ it_0 & r_0 \end{pmatrix}\begin{pmatrix} \mu_1^* \\ \mu_2^* \end{pmatrix} = -\begin{pmatrix} \mu_1 \\ \mu_2 \end{pmatrix}, \quad |\mu_1|^2 + |\mu_2|^2 = 1. \tag{3}$$

Here, we assume that the off-resonant reflection and transmission coefficients r_0 and t_0, as well as the normalized decay coefficients μ_1 and μ_2, are independent of the field intensity and the nonlinear relaxation time τ. Therefore, since these constraints hold in the small-amplitude (linear) regime, they must also hold in our nonlinear model at arbitrary intensities and characteristic nonlinear delays. Equation (3) leads to strict bounds between the parameters r_0, γ_1, and γ_2, and on the phases of μ_1, μ_2 [41].

In the instantaneous case $(\tau = 0)$, the steady-state transmissions T_{12} and T_{21} of an asymmetric system $(\gamma_1 \neq \gamma_2)$ can be markedly different in a certain range of input powers $|\xi_j^+|^2$ [11,18], as shown in Fig. 1(b) for different values of γ_2/γ_1 and fixed Δ and r_0. Sharp transitions from low to high transmission values in Fig. 1(b) are obtained by using Fano line shapes (i.e., $0 < r_0 < 1$) [42] (see caption of Fig. 1 for parameter values). The power range over which nonreciprocity occurs, termed the *nonreciprocal intensity range* (NRIR) [18], can be controlled by the degree of asymmetry γ_2/γ_1. Importantly, as shown in Ref. [18], increasing the NRIR also necessarily reduces the maximum transmission (i.e., increases the insertion loss). This is clear from comparing the different shaded regions and transmissions in Fig. 1(b). Such a bound is deeply rooted in the TR symmetry of the system, and implies that unitary transmission is only possible when the system is electromagnetically symmetric and hence reciprocal.

III. RESULTS AND DISCUSSION

A. Nonreciprocal moderate-power pulse reshaping

After having briefly summarized the nonreciprocal behavior in the instantaneous case, we now focus on the noninstantaneous nonlinear response $(\tau > 0)$. We consider a pulsed source with a duration much longer than the cavity lifetime, which is equal to $\gamma^{-1} = 1$ in our system. Figure 2 shows the normalized input pulse (black dashed line) and the corresponding transmitted profiles for excitation from either port 1 $[|\xi_2^-(t)|^2$, blue line] or port 2 $[|\xi_1^-(t)|^2$, red line], for $\gamma_2/\gamma_1 = 2$ and various values of τ, while all other parameters

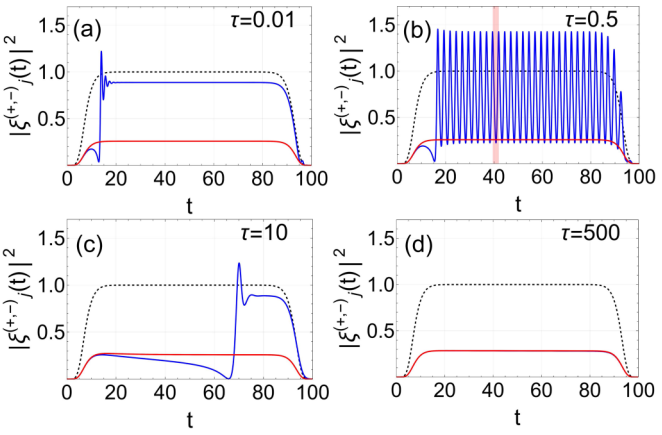

FIG. 2. Nonreciprocal response upon pulse excitation with full width at half maximum FWHM = 90 for different nonlinear relaxation times. The black dashed curves show the normalized input pulse power profile $|\xi_{1,2}^+(t)|^2$, and the solid blue (red) curves show the transmitted pulse profiles when excited from port 1 (2), $|\xi_{2,1}^-(t)|^2/P$. Parameters are the same as in Fig. 1(b) with $\gamma_2/\gamma_1 = 2$ and the peak pulse power is set to $P = 10$, which lies in the highlighted NRIR. The shaded strip in (b) highlights the calculated self-oscillation period of 2.45 in the given normalized units.

are the same as in Fig. 1(b). Following Fig. 1(b), we set the input peak power to $P \equiv |\xi_{i,\max}^+|^2 = 10$, for which the instantaneous steady-state solution (red curves) clearly exhibits large nonreciprocity. Indeed, near the instantaneous limit [$\tau = 0.01$, Fig. 2(a)] the transmission profiles are virtually identical to the ones obtained when using an instantaneous nonlinearity (not shown here), as expected, resulting in large transmission (blue) in one direction and low transmission (red) along the opposite direction. For a larger $\tau = 0.5$ [Fig. 2(b)], rapid self-oscillations appear in the highly transmitted pulse, while along the opposite direction the transmitted pulse remains virtually identical to the instantaneous limit. For longer relaxation times [$\tau = 10$, Fig. 2(c)], the self-oscillations are replaced by a nonreciprocal response largely delayed with respect to the beginning of the input pulse, resulting in significant pulse compression and reshaping combined with nonreciprocity. Finally, when the relaxation time is much longer than both pulse width and cavity lifetime [$\tau = 500$, Fig. 2(d)], reciprocity is fully restored, since the nonlinear shift of the cavity frequency is only triggered after the pulse is gone, and hence there is no mechanism to break reciprocity.

These results show that breaking TR symmetry (TRS), along with an electromagnetic asymmetry and a delayed nonlinearity, can generate highly nontrivial responses remarkably different from the instantaneous scenario. Of particular interest are the self-oscillatory dynamics shown in Fig. 2(b), which show that the system cannot reach a steady state, and are a direct consequence of TRS breaking in these systems. To obtain more insights into this response, we analyze the linear stability of (1) around the cw steady state. We make the ansatz

$$\begin{aligned} a(t) &= a_0 + \epsilon(ue^{\lambda t} + v^* e^{\lambda^* t}), \\ n(t) &= n_0 + \epsilon w(e^{\lambda t} + e^{\lambda^* t}), \end{aligned} \tag{4}$$

where $0 < \epsilon \ll 1$ and a_0 and $n_0 \equiv |a_0|^2$ are the pumping-power-dependent steady-state solutions to (1). Substituting (4)

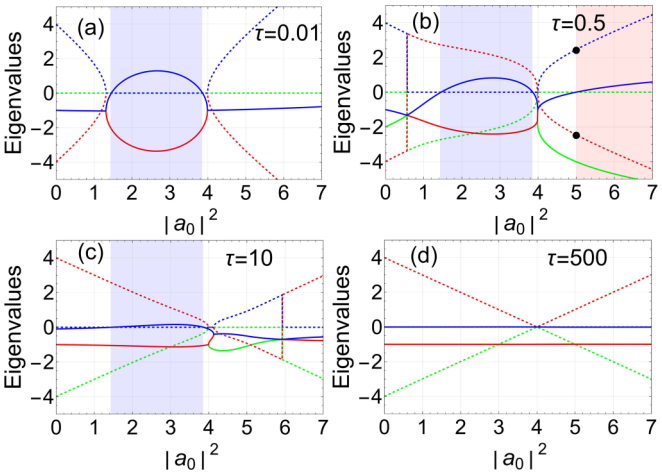

FIG. 3. Real (solid lines) and imaginary (dashed lines) parts of the three eigenvalues of system (5) (denoted by different colors or shades) as a function of steady-state intracavity energy for the same nonlinear relaxation times considered in Fig. 2. The blue shaded regions in (a)–(c) indicate a region of bistability and the red shaded region in (b) indicates the onset of self-oscillations due to a Hopf bifurcation. At the Hopf bifurcation in (b), the purely imaginary eigenvalues $\pm\lambda_H$ are indicated with black dots. The oscillation period calculated as $T_s = 2\pi/\lambda_H = 2.45$ matches well the one observed in Fig. 2(b).

into (1) and collecting terms linear in ϵ leads to

$$\lambda \begin{pmatrix} u \\ v \\ w \end{pmatrix} = \begin{pmatrix} M_0 & 0 & -ia_0 \\ 0 & M_0^* & ia_0^* \\ a_0^*/\tau & a_0/\tau & -1/\tau \end{pmatrix} \begin{pmatrix} u \\ v \\ w \end{pmatrix}, \tag{5}$$

where $M_0 = i(\Delta - |a_0|^2) - 1$. The eigenvalues of this system versus $|a_0|^2$ are shown in Fig. 3, for the same parameter values used in Fig. 2. In the nearly instantaneous limit [$\tau = 0.01$, Fig. 3(a), compare also with Fig. 2(a)] the eigenvalues are virtually identical to the ones of the 2×2 instantaneous version of (5), with a region of instability shown in the blue shaded region where the real part of a simple eigenvalue crosses zero and becomes positive over a finite range of $|a_0|^2$ values. In terms of the pumping power, this unstable region corresponds to the middle branch of the well-known S-shaped steady-state bistability curve [12]. Importantly, the imaginary part of the unstable eigenvalue (in blue) is identically zero in the bistability region shown in Fig. 3(a), which precludes self-oscillatory behavior in the instantaneous limit. In contrast, Figs. 2(b) and 3(b) show a totally different self-oscillatory dynamic when a longer delayed nonlinearity is considered. Figure 3(b) still shows a region of bistability (blue shaded region), but the real parts of two eigenvalues (red and blue curves) become identical after the bistability region and cross zero again at $|a_0|^2 = 5$, leading to instability. Unlike the instability described earlier and arising in the bistability region, here the zero-crossing eigenvalues have nonzero conjugate imaginary parts, causing a Hopf bifurcation [red shaded area in Fig. 3(b)]. The consequence can be clearly seen in Fig. 2(b), with the onset of rapid self-oscillations in the dominantly transmitted signal. The period of these self-oscillations T_s can be calculated from the magnitude of the purely imaginary eigenvalues at the Hopf bifurcation [marked in Fig. 3(b) with black dots], leading to

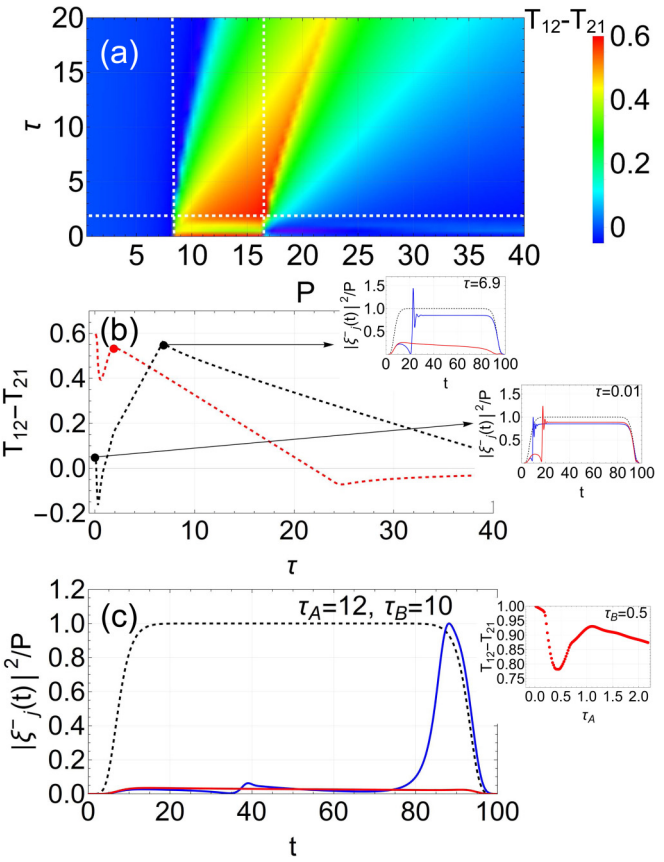

FIG. 4. (a) Nonreciprocal contrast $T_{12} - T_{21}$, for the same parameters used in Fig. 3, as a function of peak input power P and nonlinear delay τ. (b) Slices of (a) for fixed $P = 12$ (red dashed) and $P = 17.5$ (black dashed). Insets: Transmitted pulse profiles at indicated points. (c) Normalized transmitted pulses for a cascaded two-resonator system, for $\Delta_A = \Delta_B = 4$, $r_A = 0.7$, $r_B = 0.2$, and delay phase $\theta = \pi/4$ and with the same color scheme used in Fig. 2, showing a highly nonreciprocal response where the dominantly transmitted pulse is compressed to less that one-tenth the duration of the incident pulse. Inset: $T_{12} - T_{21}$ as a function of τ_A for a fixed P and $\tau_B = 0.5$, showing a similar behavior as observed for the single-resonator $P = 12$ curve in (b), but with unitary transmission as $\tau_A \to 0$.

$T_s \approx 2.45$ which agrees well with the period extracted from the numerical calculations in Fig. 2(b). The Hopf bifurcation is no longer present for $\tau = 10$ [Fig. 3(c)], which results in a lack of sustained self-oscillations in Fig. 2(c) and is discussed further below. Finally, Fig. 3(d) shows that, for nonlinear delays much longer than the pulse duration, both regions of instability effectively vanish, leading to reciprocal propagation [Fig. 2(d)].

Further insights can be obtained by studying how the delayed nonlinearity affects the total pulse transmission, defined as the ratio of total output to input energy, i.e., $T_{ij} = \int |\xi_j^-(t)|^2 dt / \int |\xi_i^+(t)|^2 dt$. Figure 4(a) shows the difference in transmission $T_{12} - T_{21}$ as a function of τ and peak power of the impinging pulse P while keeping all other parameters as in Figs. 2 and 3. The vertical white dashed lines mark the edges of the NRIR in the instantaneous limit ($\tau = 0$). We find that, as the nonlinearity delay increases, the NRIR increases, albeit with a reduced contrast, and the boundaries of the NRIR be-

come less well defined. This is more clearly seen in Fig. 4(b) for fixed $P = 12$ (red) and $P = 17.5$ (black). The insets in Fig. 4(b) show the transmitted pulse profiles for $P = 17.5$ in the instantaneous limit $\tau = 0$ (highly reciprocal) and for the optimal value of $\tau \approx 6.9$ for which nonreciprocity is maximized. This clearly shows how particular nonzero values of the delay τ allow for highly nonreciprocal behavior at power levels for which the instantaneous system would be nearly reciprocal. Furthermore, in the case $P = 12$ in Fig. 4(b), we find that even though maximum nonreciprocity is achieved near $\tau = 0$, there exists a local maximum in the nonreciprocal contrast for a nonzero critical delay, $\tau_p \approx 1.9$ [red dot in Fig. 4(b)].

Following Ref. [31], in the case of cw pumping it can be shown that the presence of self-oscillations, due to the Hopf bifurcation discussed above, disappears for nonlinear relaxation times $\tau > \tau_c$, where τ_c is the positive real root of

$$\tau_c^3 + \tau_c^2 - \left(1 + \frac{\Delta^2}{4}\right)\tau_c - 1 = 0. \tag{6}$$

For $\Delta = 4$, $\tau_c \approx 1.9$, which agrees well with what is observed in Fig. 4(b). Indeed, we can attribute the dip in nonreciprocal contrast in the $P = 12$ curve for $\tau < \tau_p$ to the onset of self-oscillations, leading to a smaller integrated value of the dominantly transmitted signal. It can be seen from Fig. 4(a), where the horizontal white dashed line is at τ_c, that the dip in nonreciprocity, for $\tau < \tau_c$ approximately holds for all P in the instantaneous NRIR. We note here that to accurately integrate these highly oscillatory signals, a temporal resolution sufficiently smaller than their period must be used ($\Delta t \sim 0.01$ in Fig. 4).

Having thoroughly analyzed the effect a delayed nonlinearity has on nonreciprocal transmission, defined by T_{ij}, we now show that a delayed nonlinearity can also be exploited to reshape and compress an incident pulse with a high nonreciprocal contrast, as measured by the transmitted pulse's peak power along opposite directions. This effect can already be observed in Fig. 2(c), although with a relatively small contrast between transmission in the two directions. Pulse compression with a much larger nonreciprocal contrast can be obtained by extending our model to include two spatially separated resonators, with different nonlinear relaxation times τ_A and τ_B and coupled via a delay line imparting a fixed phase delay θ (see the Appendix for details), Indeed, in the identically instantaneous case ($\tau_A = \tau_B = 0$), it was shown [16] that such a configuration can be tailored to exhibit unitary transmission over a finite power range still preserving the nonreciprocal response, which is not possible in the case of a single resonator due to TR symmetry. Figure 4(c) shows how this system, properly tailored, can generate a highly nonreciprocal response and simultaneous pulse compression: The pulse transmitted along one direction has the same peak power as the input pulse's, and it is compressed in time by a factor $\sim$10, while virtually no signal is transmitted along the other direction. The inset in Fig. 4(c) shows the integrated pulse transmission for such a system as a function of τ_A and for a fixed $\tau_B = 0.5$. Here, the dip shown in nonreciprocal contrast is very similar to the one observed in Figs. 4(a) and 4(b), due to self-oscillations, but with a higher contrast that becomes unitary in the instantaneous limit. Even though there exist transient dynamics when considering an instantaneous nonlinearity, where nonreciprocity can differ substantially from the cw case, these transient effects depend only on the resonator's frequency and linewidth. Importantly, the ability to control the nonreciprocal response freely over the pulse duration, as exhibited in the main plot in Fig. 4(c), is only possible by utilizing a delayed nonlinear response.

B. High-power nonreciprocal cw modulation: Chaotic regime

In this section we investigate the nonreciprocal dynamics of a single cavity when excited by a cw signal which is detuned far off resonance. Note that in this regime the steady-state bistability region occurs for much higher input powers [11]. Our goal here is not to optimize the nonreciprocal contrast, but to show that, when the resonator's characteristic nonlinear delay is on the same order as the cavity lifetime and the source is tuned far from the resonator's bare frequency, it is possible to tailor a periodic or chaotic modulation of the source in a highly nonreciprocal manner.

In Fig. 5, we fix the resonator asymmetry to $\gamma_2/\gamma_1 = 2$, the detuning to $\Delta = 15$, and the characteristic delay at $\tau = 0.35$. In this regime, we expect the onset of chaotic behavior in the dynamics described by (1) near the bistable switching points, due to the destabilization of limit cycles [27,31]. The main plot in Fig. 5 tracks the period-doubling bifurcation route to chaos as the input power is decreased from port 1 (blue) and port 2 (red). The vertical axis shows the corresponding output power when the intracavity amplitude $a(t)$ is at the fixed phase where the imaginary part of $a(t) = 0$ (over sufficiently long times so that transient dynamics are not included). As expected, we find the emergence of periodic and chaotic windows in the output power. The main plot in Fig. 5 shows that,

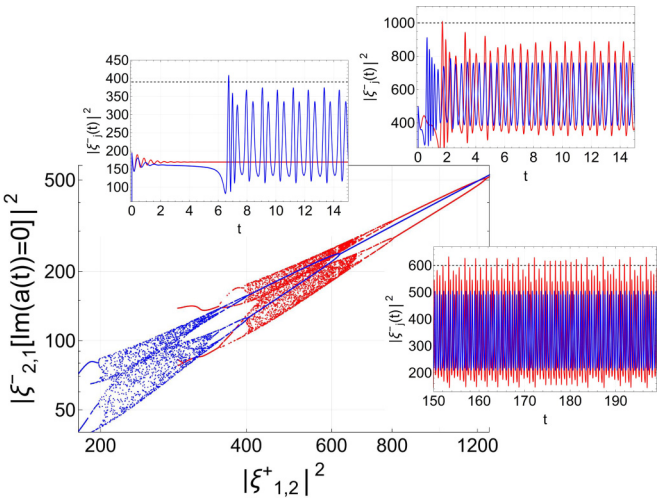

FIG. 5. A single resonator with $\Delta = 15$, $\tau = 0.35$, and $\gamma_2/\gamma_1 = 2$. The main plot is the transmitted output power for a fixed phase intracavity amplitude (set by $\mathrm{Im}[a(t)] = 0$) at long times as a function of the input power when sourced from port 1 (blue) or port 2 (red). Regions of chaos due to a period-doubling bifurcation among periodic windows are seen. The insets show corresponding temporal modulations with the same color scheme at the input powers shown in the black dashed lines.

due to the asymmetry, these windows may be tailored in such a way as to induce a desired nonreciprocal modulation of the signal. Indeed, the insets in Fig. 5 show possible nonreciprocal modulations at different input powers. The upper-left-hand inset ($P = 390$) shows a scenario where the initial intracavity amplitude is zero and along one direction the output eventually settles into a stable doubly periodic limit cycle, whereas in the opposite direction the output approaches a stable fixed point. Similarly, the upper-right-hand inset ($P = 1000$) shows, after a brief transient dynamic of aperiodic oscillations, steady periodic and doubly periodic modulations in opposing directions. Finally, the lower-right-hand inset ($P = 600$) shows, for an initial intracavity amplitude determined using the main bifurcation diagram, a deterministic chaotic modulation in one direction, contrasted by a doubly periodic modulation in the other.

In Ref. [32] it was proposed that a chaotic resonator could be used as a detector for a weak laser signal from a remote source in the presence of strong background noise, by detecting large qualitative changes in the resonator's dynamics due to small changes in resonant power injection. One possible application of the nonreciprocal chaotic regime demonstrated here would be the additional directional feature added to such a detector.

IV. CONCLUSION

We have shown that the inclusion of noninstantaneous nonlinearities combined with spatial asymmetries opens remarkable opportunities to tailor the nonreciprocal response of passive, bias-free resonant systems, leading to different practical functionalities, including pulse shaping, compression, and self-oscillatory responses. Besides demonstrating these functionalities, we also verified that large nonlinearity-induced nonreciprocity can be obtained also in the case of slow nonlinear responses. This is very important in practical scenarios, since often materials characterized by slower nonlinearities, such as carrier injection or thermo-optical effects, are utilized for nonreciprocal devices. Furthermore, we have shown that the nonreciprocal contrast of such functionalities can be greatly increased by coupling together multiple resonators. In the high-detuning regime we have shown that it is possible to engineer the asymmetry and characteristic delay of a single resonator to generate nonreciprocal chaotic dynamics. Achieving such advanced control over highly nonreciprocal cw and pulse shaping would be of great interest for a variety of classical and quantum photonic scenarios.

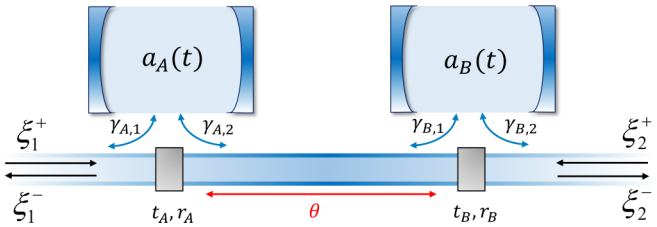

FIG. 6. Schematic of the considered two-port, two-resonator (A and B) asymmetric and noninstantaneous nonlinear system with a phase delay θ.

ACKNOWLEDGMENTS

This work was supported by the Simons Foundation, the Air Force Office of Scientific Research MURI program with Grant No. FA9550-18-1-0379, and the Office of Naval Research with Grant No. N00014-19-1-2011.

APPENDIX: COUPLED TWO-RESONATOR MODEL

We model two cascaded noninstantaneous nonlinear resonators coupled by a constant phase shift θ, shown schematically in Fig. 6, by the equations [11]

$$\frac{d\mathbf{a}}{dt} = M\mathbf{a} + K^T\boldsymbol{\xi}^+, \quad \tau_{A,B}\frac{dn_{A,B}}{dt} + n_{A,B} = |a_{A,B}|^2,$$
$$\boldsymbol{\xi}^- = K\mathbf{a} + C\boldsymbol{\xi}^+, \tag{A1}$$

where $\mathbf{a} = (a_A, a_B)^T$ are the separated resonance amplitudes, $\boldsymbol{\xi}^{\pm} = (\xi_1^{\pm}, \xi_2^{\pm})^T$ are the input/output fields at the two ports, τ_A and τ_B are the individual nonlinear relaxation times, and the matrices M, K, and C are given by

$$M = \begin{pmatrix} i(\Delta_A - n_A(t)) - 1 + \dfrac{\sqrt{2}\mu_{A,2}^2 r_B e^{i\theta}}{e^{2i\theta} - r_A r_B} & \dfrac{\sqrt{2}\mu_{A,2}\mu_{B,1}}{e^{2i\theta} - r_A r_B} \\ \dfrac{\sqrt{2}\mu_{A,2}\mu_{B,1}}{e^{2i\theta} - r_A r_B} & i(\Delta_B - n_B(t)) - 1 + \dfrac{\sqrt{2}\mu_{B,1}^2 r_A e^{i\theta}}{e^{2i\theta} - r_A r_B} \end{pmatrix}, \tag{A2}$$

$$K = \sqrt{2}\begin{pmatrix} \mu_{A,1} + \dfrac{i\mu_{A,2} r_B t_A}{e^{2i\theta} - r_A r_B} & \dfrac{ie^{i\theta}\mu_{B,1} t_A}{e^{2i\theta} - r_A r_B} \\ \dfrac{ie^{i\theta}\mu_{A,2} t_B}{e^{2i\theta} - r_A r_B} & \mu_{B,2} + \dfrac{i\mu_{B,1} r_A t_B}{e^{2i\theta} - r_A r_B} \end{pmatrix}, \quad C = \begin{pmatrix} r_A - \dfrac{t_A^2 r_B}{e^{2i\theta} - r_A r_B} & -\dfrac{e^{i\theta} t_A t_B}{e^{2i\theta} - r_A r_B} \\ -\dfrac{e^{i\theta} t_A t_B}{e^{2i\theta} - r_A r_B} & r_B - \dfrac{t_B^2 r_A}{e^{2i\theta} - r_A r_B} \end{pmatrix}. \tag{A3}$$

In the expressions above, $\Delta_{A,B}$ are the individual detunings of the resonators, $(r_{A,B}, t_{A,B})$ are the off-resonant reflection and transmission coefficients of each separate resonator, and $(\mu_{A,j}, \mu_{B,j})$ $(j = 1, 2)$ are the individual coupling parameters to the ports. Importantly, the matrices above satisfy the time-reversibility condition $CK^* = -K$. Again, since we assume that the entries in C and K are independent of field intensities and the characteristic nonlinear relaxation times, these constraints continue to hold even though the inclusion of a noninstantaneous nonlinearity explicitly breaks the overall time-reversal symmetry of our model.

[1] R. E. Collin, *Antennas and Radiowave Propagation* (McGraw-Hill, New York, 1985).

[2] L. Bi, J. Hu, P. Jiang, D. H. Kim, G. F. Dionne, L. C. Kimerling, and C. Ross, On-chip optical isolation in monolithically integrated non-reciprocal optical resonators, Nat. Photonics **5**, 758 (2011).

[3] Y. Zhang, Q. Du, C. Wang, T. Fakhrul, S. Liu, L. Deng, D. Huang, P. Pintus, J. Bowers, C. A. Ross *et al.*, Monolithic integration of broadband optical isolators for polarization-diverse silicon photonics, Optica **6**, 473 (2019).

[4] Z. Yu and S. Fan, Complete optical isolation created by indirect interband photonic transitions, Nat. Photonics **3**, 91 (2009).

[5] K. Fang, Z. Yu, and S. Fan, Realizing effective magnetic field for photons by controlling the phase of dynamic modulation, Nat. Photonics **6**, 782 (2012).

[6] K. Fang, Z. Yu, and S. Fan, Photonic Aharonov-Bohm Effect Based on Dynamic Modulation, Phys. Rev. Lett. **108**, 153901 (2012).

[7] H. Lira, Z. Yu, S. Fan, and M. Lipson, Electrically Driven Nonreciprocity Induced by Interband Photonic Transition on a Silicon Chip, Phys. Rev. Lett. **109**, 033901 (2012).

[8] D. L. Sounas, C. Caloz, and A. Alu, Giant non-reciprocity at the subwavelength scale using angular momentum-biased metamaterials, Nat. Commun. **4**, 2407 (2013).

[9] D. B. Sohn, S. Kim, and G. Bahl, Time-reversal symmetry breaking with acoustic pumping of nanophotonic circuits, Nat. Photonics **12**, 91 (2018).

[10] D. L. Sounas and A. Alù, Non-reciprocal photonics based on time modulation, Nat. Photonics **11**, 774 (2017).

[11] M. Cotrufo, S. A. Mann, H. Moussa, and A. Alù, Nonlinearity-induced nonreciprocity–Part I, IEEE Trans. Microwave Theory Tech. **69**, 3569 (2021).

[12] R. Boyd, *Nonlinear Optics*, 4th ed. (Elsevier, Amsterdam, 2020).

[13] L. Fan, J. Wang, L. T. Varghese, H. Shen, B. Niu, Y. Xuan, A. M. Weiner, and M. Qi, An all-silicon passive optical diode, Science **335**, 447 (2011).

[14] K. Y. Yang, J. Skarda, M. Cotrufo, A. Dutt, G. H. Ahn, M. Sawaby, D. Vercruysse, A. Arbabian, S. Fan, A. Alù *et al.*, Inverse-designed non-reciprocal pulse router for chip-based lidar, Nat. Photonics **14**, 369 (2020).

[15] Y. Yu, Y. Chen, H. Hu, W. Xue, K. Yvind, and J. Mork, Nonreciprocal transmission in a nonlinear photonic-crystal Fano structure with broken symmetry, Laser Photonics Rev. **9**, 241 (2015).

[16] D. L. Sounas, J. Soric, and A. Alù, Broadband passive isolators based on coupled nonlinear resonances, Nat. Electron. **1**, 113 (2018).

[17] Y. Pan, C. Wang, Z. Lyu, and T. Chen, Nonlinearity-induced asymmetric diffraction in a hybrid A/B structure with two azo-containing materials, Appl. Phys. Lett. **118**, 011108 (2021).

[18] D. L. Sounas and A. Alù, Fundamental bounds on the operation of Fano nonlinear isolators, Phys. Rev. B **97**, 115431 (2018).

[19] M. Lawrence, D. R. Barton, and J. A. Dionne, Nonreciprocal flat optics with silicon metasurfaces, Nano Lett. **18**, 1104 (2018).

[20] B. Jin and C. Argyropoulos, Self-Induced Passive Nonreciprocal Transmission by Nonlinear Bifacial Dielectric Metasurfaces, Phys. Rev. Applied **13**, 054056 (2020).

[21] A. Mekawy, D. L. Sounas, and A. Alù, Free-space nonreciprocal transmission based on nonlinear coupled Fano metasurfaces, Photonics **8**, 139 (2021).

[22] C. Müller, J. Combes, A. R. Hamann, A. Fedorov, and T. M. Stace, Nonreciprocal atomic scattering: A saturable, quantum Yagi-Uda antenna, Phys. Rev. A **96**, 053817 (2017).

[23] A. Rosario Hamann, C. Müller, M. Jerger, M. Zanner, J. Combes, M. Pletyukhov, M. Weides, T. M. Stace, and A. Fedorov, Nonreciprocity Realized with Quantum Nonlinearity, Phys. Rev. Lett. **121**, 123601 (2018).

[24] Q. Lin, O. J. Painter, and G. P. Agrawal, Nonlinear optical phenomena in silicon waveguides: Modeling and applications, Opt. Express **15**, 16604 (2007).

[25] Z. Geng, K. J. H. Peters, A. A. P. Trichet, K. Malmir, R. Kolkowski, J. M. Smith, and S. R. K. Rodriguez, Universal Scaling in the Dynamic Hysteresis, and Non-Markovian Dynamics, of a Tunable Optical Cavity, Phys. Rev. Lett. **124**, 153603 (2020).

[26] G. Keijsers, Z. Geng, K. J. H. Peters, M. Wouters, and S. R. K. Rodriguez, Steady-state superfluidity of light in a tunable cavity at room temperature, arXiv:2012.13463.

[27] K. Ikeda, H. Daido, and O. Akimoto, Optical Turbulence: Chaotic Behavior of Transmitted Light from a Ring Cavity, Phys. Rev. Lett. **45**, 709 (1980).

[28] N. Cazier, X. Checoury, L.-H. Haret, and P. Boucaud, High-frequency self-induced oscillations in a silicon nanocavity, Opt. Express **21**, 13626 (2013).

[29] D. M. Abrams, A. Slawik, and K. Srinivasan, Nonlinear Oscillations and Bifurcations in Silicon Photonic Microresonators, Phys. Rev. Lett. **112**, 123901 (2014).

[30] K. Ikeda and O. Akimoto, Instability Leading to Periodic and Chaotic Self-Pulsations in a Bistable Optical Cavity, Phys. Rev. Lett. **48**, 617 (1982).

[31] A. Armaroli, S. Malaguti, G. Bellanca, S. Trillo, A. de Rossi, and S. Combrie, Oscillatory dynamics in nanocavities with noninstantaneous Kerr response, Phys. Rev. A **84**, 053816 (2011).

[32] W. W. Chow and S. Wieczorek, Using chaos for remote sensing of laser radiation, Opt. Express **17**, 7491 (2009).

[33] A. Argyris, D. Syvridis, L. Larger, V. Annovazzi-Lodi, P. Colet, I. Fischer, J. Garcia-Ojalvo, C. R. Mirasso, L. Pesquera, and K. A. Shore, Chaos-based communications at high bit rates using commercial fibre-optic links, Nature (London) **438**, 434 (2005).

[34] K. M. Cuomo, A. V. Oppenheim, and S. H. Strogatz, Synchronization of Lorenz-based chaotic circuits with applications to communications, IEEE Trans. Circuits Syst. II **40**, 626 (1993).

[35] S. Lepri and A. Pikovsky, Nonreciprocal wave scattering on nonlinear string-coupled oscillators, Chaos **24**, 043119 (2014).

[36] D.-W. Zhang, L.-L. Zheng, C. You, C.-S. Hu, Y. Wu, and X.-Y. Lu, Nonreciprocal chaos in a spinning optomechanical resonator, Phys. Rev. A **104**, 033522 (2021).

[37] H. Mori, Transport, collective motion, and Brownian motion, Prog. Theor. Phys. **33**, 423 (1965).

[38] P. Hänggi, Correlation functions and mastere quations of generalized (non-Markovian) Langevin equations, Z. Phys. B **31**, 407 (1978).

[39] K. Peters and S. Rodriguez, Limit cycles and chaos induced by a nonlinearity with memory, arXiv:2108.02680.

[40] S. Fan, W. Suh, and J. D. Joannopoulos, Temporal coupled-mode theory for the Fano resonance in optical resonators, J. Opt. Soc. Am. A **20**, 569 (2003).

[41] K. X. Wang, Z. Yu, S. Sandhu, and S. Fan, Fundamental bounds on decay rates in asymmetric single-mode optical resonators, Opt. Lett. **38**, 100 (2013).

[42] X. Yang, C. Husko, C. W. Wong, M. Yu, and D. L. Kwong, Observation of femtojoule optical bistability involving Fano resonances in high Q/V_m silicon photonic crystal nanocavities, Appl. Phys. Lett. **91**, 051113 (2007).